THE JOURNAL OF BIOLOGICAL CHEMISTRY VOL. 288, NO. 20, pp. 14497–14509, May 17, 2013

Angiotensin II Impairs Endothelial Nitric-oxide Synthase Bioavailability under Free Cholesterol-enriched Conditions via Intracellular Free Cholesterol-rich Membrane Microdomains*[S]

Received for publication, January 13, 2013, and in revised form, March 29, 2013 Published, JBC Papers in Press, April 2, 2013, DOI 10.1074/jbc.M112.448522

Eisuke Amiya[‡], Masafumi Watanabe[‡], Norihiko Takeda[‡], Tetsuya Saito[‡], Taro Shiga[‡], Yumiko Hosoya[‡], Tomoko Nakao[‡], Yasushi Imai[‡], Ichiro Manabe[‡], Ryozo Nagai[‡§], Issei Komuro[‡¶], and Koji Maemura[‖1]

From the [‡]Department of Cardiovascular Medicine, Graduate School of Medicine, the University of Tokyo, Tokyo 113-8655, Japan, [§]Jichi Medical University, Shimotsuke 329-0498, Japan, the [¶]Department of Cardiovascular Medicine, Osaka University Graduate School of Medicine, Osaka 565-0871, Japan, and the [‖]Department of Cardiovascular Medicine, Nagasaki University Graduate School of Biomedical Sciences, Nagasaki 852-8102, Japan

Background: Free cholesterol forms membrane microdomains in endothelial cells.
Results: Free cholesterol loading formed intracellular vesicles with free cholesterol-rich microdomains that were shifted toward late endosomes/lysosomes by angiotensin II, resulting in impairment of endothelial NOS availability.
Conclusion: Angiotensin II decreased the bioavailability of endothelial NOS in a free cholesterol-enriched condition.
Significance: Free cholesterol-rich microdomains are crucial platforms of endothelial NOS availability.

Vascular endothelial function is impaired in hypercholesterolemia partly because of injury by modified LDL. In addition to modified LDL, free cholesterol (FC) is thought to play an important role in the development of endothelial dysfunction, although the precise mechanisms remain to be elucidated. The aim of this study was to clarify the mechanisms of endothelial dysfunction induced by an FC-rich environment. Loading cultured human aortic endothelial cells with FC induced the formation of vesicular structures composed of FC-rich membranes. Raft proteins such as phospho-caveolin-1 (Tyr-14) and small GTPase Rac were accumulated toward FC-rich membranes around vesicular structures. In the presence of these vesicles, angiotensin II-induced production of reactive oxygen species (ROS) was considerably enhanced. This ROS shifted endothelial NOS (eNOS) toward vesicle membranes and vesicles with a FC-rich domain trafficked toward perinuclear late endosomes/lysosomes, which resulted in the deterioration of eNOS Ser-1177 phosphorylation and NO production. Angiotensin II-induced ROS decreased the bioavailability of eNOS under the FC-enriched condition.

Hyperlipidemia is a major cause of endothelial dysfunction leading to atherosclerosis. One mechanism of endothelial dysfunction in hyperlipidemia is attributable to an increase in circulating LDLs (1). Furthermore, the atherogenic potential of LDLs may increase after oxidation to oxidized LDL, and the action of oxidized LDLs leads to endothelial dysfunction through a pathway mediated by the oxidized LDL receptor-1 (LOX-1) (2).

Recent studies have shown that in addition to the effect of LDLs, an increase in free cholesterol (FC)[2] may be a crucial factor contributing to endothelial dysfunction in hyperlipidemia. The earliest event in hyperlipidemia is the accumulation of plasma lipoproteins in the subendothelium of the arterial tree (3). Lipoproteins that accumulate in the subendothelium are oxidatively modified and reassembled into lipoproteins through interaction with proteoglycans and other matrix proteins (3). FC, which is abundant in these lipoproteins, is released by the action of cholesterol ester hydrolytic enzymes derived from macrophages in the extracellular spaces (4, 5). Consequently, cells located in the atherosclerotic lesions are exposed to an FC-rich extracellular environment. Extracellular FC can be directly incorporated into the plasma membranes (PMs) of cells, leading to an increase in cellular cholesterol levels (6, 7). Indeed, Fang *et al.* (8) showed that hypercholesterolemia increased the level of cellular FC ~2–4-fold in vascular endothelial cells (ECs). FC is an essential component of mem-

* This work was supported by grants from the Japan Society for the Promotion of Science through the Funding Program for World-Leading Innovative R&D on Science and Technology (FIRST Program), initiated by the Council for Science and Technology Policy. This work was also supported by Grant-in-Aid for Scientific Research 19590853 from the Ministry of Education, Science, and Culture, Japan (to K. M.) and by funds from the Takeda Science Foundation (to K. M.) and the Mitsubishi Pharma Research Foundation (to K. M.).
[S] This article contains supplemental text and Figs. S1–S7.
[1] To whom correspondence should be addressed: To whom correspondence should be addressed: Koji Maemura, Department of Cardiovascular Medicine, Nagasaki University Graduate School of Biomedical Sciences, 1-7-1 Sakamoto, Nagasaki, Japan. Tel.: 852-8501; E-mail: maemura@nagasaki-u.ac.jp.

[2] The abbreviations used are: FC, free cholesterol; Chol, cholesterol; Ang II, angiotensin II; eNOS, endothelial NOS; ROS, reactive oxygen species; PM, plasma membrane; EC, endothelial cell; MBCD, methyl-β-cyclodextrin; DPI, diphenyleneiodonium chloride; TEP, triethyl phosphate; H2DCFDA, 2′,7′-dichlorodihydrofluorescein diacetate; DAF-FM DA, diaminofluorescein-FM diacetate; Cav, caveolin; LAMP-1, lysosome-associated membrane protein-1; EEA-1, early endosome antigen-1; P-Cav, phospho-caveolin; HAEC, human aortic endothelial cell; ICQ, intensity correlation quotient.

brane lipid bilayers, and an increase in intracellular FC modulates the physical properties of biological membranes and affects the activities of membrane-bound protein complexes. In macrophages, the accumulation of excess FC leads to cell death during the process of atherosclerosis through an endoplasmic reticulum-mediated mechanism (9). In smooth muscle cells, a high level of FC was found to promote cell proliferation, leading to a proatherogenic state (10), or transdifferentiation, leading to a macrophage-like state (11). In particular, ECs have a tendency to accumulate FC rather than esterified cholesterol (12). Therefore, the effect of FC enrichment on ECs seems to be much greater compared with its effect on other cell types. The critical factor affecting intracellular cholesterol enrichment is a lipid raft microdomain. The lipid raft is defined as a microdomain enriched in FC and sphingolipids in the PM. Lipid rafts are reported to be involved in many important signaling pathways such as those of angiotensin II (Ang II), vascular endothelial growth factor, endothelial NOS (eNOS), and H_2O_2 in ECs (13, 14). In addition, hypercholesterolemia is reported to alter the composition of lipid rafts and affect cell function in smooth muscle cells (15).

Among the factors closely associated with the lipid raft microdomain, Ang II is an oligopeptide that has marked impact on the function of ECs. Ang II is involved in the production of reactive oxygen species (ROS) through NADPH oxidase activation (13), resulting in modulation of cell function. These responses are strongly regulated by the lipid raft compartment (16, 17). However, how the effect of Ang II on ECs is modified by the intracellular cholesterol condition has not been clarified precisely. In this study, we investigated how Ang II affects EC function in an FC-enriched environment, with special reference to the composition or structure of FC-rich membrane microdomains.

EXPERIMENTAL PROCEDURES

Materials—Cholesterol, *N*-acetylcysteine, methyl-β-cyclodextrin (MBCD), digitonin, filipin III, diphenyleneiodonium chloride (DPI), apocynin, and Oil Red O were obtained from Sigma. Ang II, triethyl phosphate (TEP), PD123319, and 4% paraformaldehyde were obtained from Wako (Tokyo, Japan). OptiPrep, 2′,7′-dichlorodihydrofluorescein diacetate (H2DCFDA), and diaminofluorescein-FM diacetate (DAF-FM DA) were purchased from Daiichi Pure Chemicals Co. (Tokyo, Japan). Polyclonal antibodies against human caveolin-2 (Cav-2) and monoclonal antibodies against human Golgin 97 and human lysosome-associated membrane protein-1 (LAMP-1) were purchased from Molecular Probes, Inc. (Carlsbad, CA). Polyclonal antibodies against human eNOS was purchased from BD Biosciences. Polyclonal antibodies against human phospho-eNOS (Ser-1177) (p-eNOS), heat shock protein 90 (Hsp90), Rab7, Rac1/2/3, caveolin-1 (Cav-1), early endosome antigen-1 (EEA-1), and phospho-caveolin-1 (Tyr-14) (P-Cav-1) were purchased from Cell Signaling Technology (Beverly, MA). Millex GV filter units (0.22 μm) were purchased from Millipore (Billerica, MA). Alexa 546-conjugated phalloidin, Alexa 488- and Alexa 594-conjugated anti-rabbit IgG, Alexa 488-conjugated anti-mouse IgG, and Hoechst 33258 pentahydrate were purchased from Invitrogen. BCA protein assay kits were obtained from Pierce. The cholesterol quantitation kit was purchased from BioVision (Mountain View, CA). Olmesartan was kindly provided by Daiichisankyo (Tokyo, Japan).

Cell Culture—Human aortic endothelial cells (HAECs) were purchased from BioWhittaker (Walkersville, MD) and maintained in EGM-2 medium (BioWhittaker) at 37 °C in a humidified atmosphere of 5% CO_2. The cells were used between passages 6 and 10 at a subconfluent stage. They were starved in EBM-2 medium supplemented with 0.5% FBS for 8–12 h before each procedure.

Fluorescence Microscopy and Antibodies—HAECs were grown on coverslips, washed with PBS, and fixed with 4% paraformaldehyde or 4% paraformaldehyde with 0.1% glutaraldehyde in PBS for 30 min, after which the fixative was rinsed with PBS and quenched with 50 mmol/liter glycine in PBS. The cells were then permeabilized with 0.5% Triton X-100 for 5 min or 0.01% digitonin for 5–20 min. As appropriate, a chemical antigen retrieval step was added to improve immunolabeling efficiency using 0.5% SDS in PBS for 5 min (18). After blocking, the cells were incubated with primary antibodies followed by the appropriate fluorescence-labeled secondary antibodies. F-actin was labeled using Alexa 546-conjugated phalloidin. The cell nuclei were labeled with Hoechst 33258 for 5 min. The coverslips were viewed and evaluated with an LSM 510 confocal microscope. Co-localization analysis was performed through intensity correction analysis with Image J. Intensity correction analysis tests whether intensities in two channels vary in a parallel, independent, or segregated manner, corresponding to co-localization, random distribution, or exclusion of red and green signals, respectively (19). Based on the algorithm, in an image where the intensities vary together (*i.e.*, both channel intensities are above or below the mean), the product of the differences from the mean will be positive. If the pixel intensities vary asynchronously (*e.g.*, the intensity of one channel is above its mean, whereas the intensity of the other channel is below its mean), then most of the product of the differences from the mean will be negative. The intensity correlation quotient (ICQ) is equal to the ratio of the number of positive product of the differences from the mean values to the total number of pixel values. The ICQ values are distributed between −0.5 and +0.5 by subtracting 0.5 from this ratio (random staining: ICQ = 0; segregated staining: $0 > \text{ICQ} > -0.5$; dependent staining: $0 < \text{ICQ} < +0.5$).

Modulation of Cellular Cholesterol Level—We used MBCD saturated with cholesterol (Chol/MBCD) to increase the intracellular FC content in the cultured HAECs (20). Chol/MBCD was produced at an MBCD:cholesterol molar ratio of 100:1 by adding 15 mg of cholesterol to 500 mg of MBCD dissolved in 10 ml of water. The mixture was rotated overnight at 37 °C, and the resulting clear solution was freeze-dried. The freeze-dried product was stored at 4 °C. Forty microliters of Chol/MBCD was added to 1 ml of medium, yielding an MBCD concentration of 2 mmol/liter in each experiment.

ROS Detection—Production of ROS and reactive nitrogen species was measured with the fluorescent dye H2DCFDA, which detects H_2O_2, peroxyl radicals, and peroxynitrite anions. HAECs were incubated with 10 μmol/liter H2DCFDA for 20

min at 37 °C. Subsequently, the cells were washed and stimulated with Ang II and Chol/MBCD and observed by fluorescence microscopy with an FITC filter.

NO Measurements—The cell-permeable NO indicator DAF-FM DA was used to measure NO. DAF-FM DA was dissolved in Me_2SO to obtain a 10 mmol/liter stock solution. HAECs were incubated with 10 μmol/liter DAF-FM DA for 20 min at 37 °C. Subsequently, the cells were washed and stimulated with Ang II and Chol/MBCD and observed using fluorescence microscopy with an FITC filter.

Western Blot Analysis—The lysis buffer contained 25 mmol/liter Tris, 10 mmol/liter EDTA, 10 mmol/liter EGTA, 1 mmol/liter sodium orthovanadate, 10 mmol/liter sodium pyrophosphate, 100 mmol/liter sodium fluoride, 1% Triton X-100, and 1 mmol/liter PMSF (pH 7.4) and was supplemented with a complete protease inhibitor mixture (Roche Applied Science). The samples were subjected to SDS-PAGE on 8.5% gels and then blotted onto nitrocellulose. After labeling with the primary and secondary antibodies, the proteins were visualized using an ECL chemiluminescence kit (Amersham Biosciences).

SDS-resistant eNOS dimers and monomers were separated by low temperature SDS-PAGE. In brief, the samples were subjected to SDS-PAGE without boiling, and gels and buffers were maintained at 4 °C during the procedure (21, 22).

Measurements of Intracellular Cholesterol Content after Modulation—Cellular cholesterol content was measured using a cholesterol quantitation kit (BioVision, Mountain View, CA). Cholesterol ester hydrolase was added when estimating total cholesterol levels but not when estimating FC. The cholesterol content was normalized according to the protein concentration measured using the BCA kit.

Filipin Fluorescence Staining of FC—Cells were fixed with 4% paraformaldehyde in PBS for 1 h at room temperature. Paraformaldehyde was rinsed with PBS and quenched with 50 mmol/liter glycine in PBS. The cells were incubated for 2 h at room temperature in PBS containing 0.05 mg/ml filipin added from a stock solution in Me_2SO. After washing, the cells were observed using an LSM 510 confocal microscope with a UV filter set.

Oil Red O Staining—Vesicle structures were examined by Oil Red O staining. Oil Red O/TEP stock was prepared by dissolving 500 mg of Oil Red O in 60 ml of TEP and 40 ml of distilled water (23). Prior to staining, a 36% TEP working solution containing 12 ml of Oil Red O/TEP stock and 8 ml of distilled water were prepared. This solution was filtered through a PVDF membrane filter (0.22 μm). After fixation, the cells were rinsed, and the 36% TEP solution was applied for 1 min. Next, the cells were incubated with Oil Red O/TEP solution for 15 min followed by rinsing with 36% TEP and PBS. They were observed under a differential interference contrast microscope and an LSM 510 confocal microscope using a Texas Red filter.

Analysis of Lipid Rafts by Density Gradient Centrifugation—After rinsing twice with ice-cold PBS, the cells were extracted in lysis buffer (25 mmol/liter Tris, 150 mmol/liter sodium chloride, 10 mmol/liter EDTA, 10 mmol/liter EGTA, 1 mmol/liter sodium orthovanadate, 10 mmol/liter sodium pyrophosphate, 100 mmol/liter sodium fluoride, 1% Triton X-100, 1 mmol/liter PMSF, pH 7.4) and complete protease inhibitor mixture (Roche Applied Science) and homogenized by passing through a 26-gauge needle 10 times. The samples were incubated at 4 °C for 20 min, and the postnuclear supernatant was recovered after centrifugation at 1000 × *g* at 4 °C for 10 min. OptiPrep 60% was added to the lysate supernatant (0.6 ml) at the bottom of an ultracentrifuge tube (SW55Ti; Beckman, Munich, Germany) to obtain a final concentration of 40%. A layer of 1.3 ml of OptiPrep 30% (OptiPrep 60% diluted in OptiPrep buffer containing 0.25 mol/liter sucrose, 20 mmol/liter Tris, and 1 mmol/liter EDTA) and a final layer of 1.3 ml of OptiPrep 15% were added. After centrifugation at 100,000 × *g* for 7 h at 4 °C, the content of each tube was fractionated from top to bottom into nine fractions of 0.5 ml each. Identical volumes of each fraction were analyzed by SDS-PAGE and immunoblotting. Insoluble lipid rafts have a lower buoyant density and float to the interface between the 30 and 15% OptiPrep layers (between fractions 6 and 7).

Electron Microscopy—HAECs were cultured in 100-mm dishes and fixed for 12 h with 4% paraformaldehyde and 25% glutaraldehyde in PBS at room temperature and postfixed with 4% osmium tetroxide in cacodylate buffer, dehydrated in graded alcohol series, and embedded in Epon for thin sectioning. Ultrathin sections were cut and stained with uranyl acetate and lead citrate and examined using a Hitachi H-7000 transmission electron microscopy at 75 kV. The solubilized filipin was added to the 4% paraformaldehyde, 25% glutaraldehyde fixative at 0.05 mg/ml and incubated for 2 h before osmium tetroxide fixation to visualize the FC-rich compartments (24).

RESULTS

Biogenesis of Vesicle Structures—Loading with Chol/MBCD is commonly used to evaluate the effects of cellular FC enrichment (10, 20). Administration of Chol/MBCD increased the intracellular FC content in cultured HAECs. Total cholesterol gradually increased 2-fold within 60 min after incubation with Chol/MBCD (Fig. 1*A*). The FC content increased 6–8-fold within 60 min. This intracellular FC concentration was similar to that observed in ECs in hypercholesterolemia (8).

Next, we examined the morphological changes in ECs by Oil Red O staining. After Chol/MBCD loading for 1 h, Oil Red O-stained vesicle structures with diameters of 0.5–1 μm were produced in the cytoplasm of HAECs (Fig. 1*B*), and it increased in a time- and dose-dependent manner (data not shown). Filipin staining, which can determine the subcellular localization of FC, also showed formations of similar vesicle structures intracellularly after Chol/MBCD loading (Fig. 1*C*, *panels b*, *d*, and *e*), whereas filipin staining was mainly localized within plasma membrane in control conditions (Fig. 1*C*, *panels a* and *c*). Co-staining with Oil Red O and filipin showed that filipin staining was at the periphery of vesicle structures; therefore, vesicle structures visualized by Oil Red O staining were composed of FC-rich phospholipid membranes (Fig. 1*D*). Electron microscopic analysis demonstrated that multivesicular bodies with similar diameters increased markedly after Chol/MBCD loading (Fig. 1*E* and supplemental Fig. S1). Filipin staining modified the outer and intraluminal membranes of the multi-

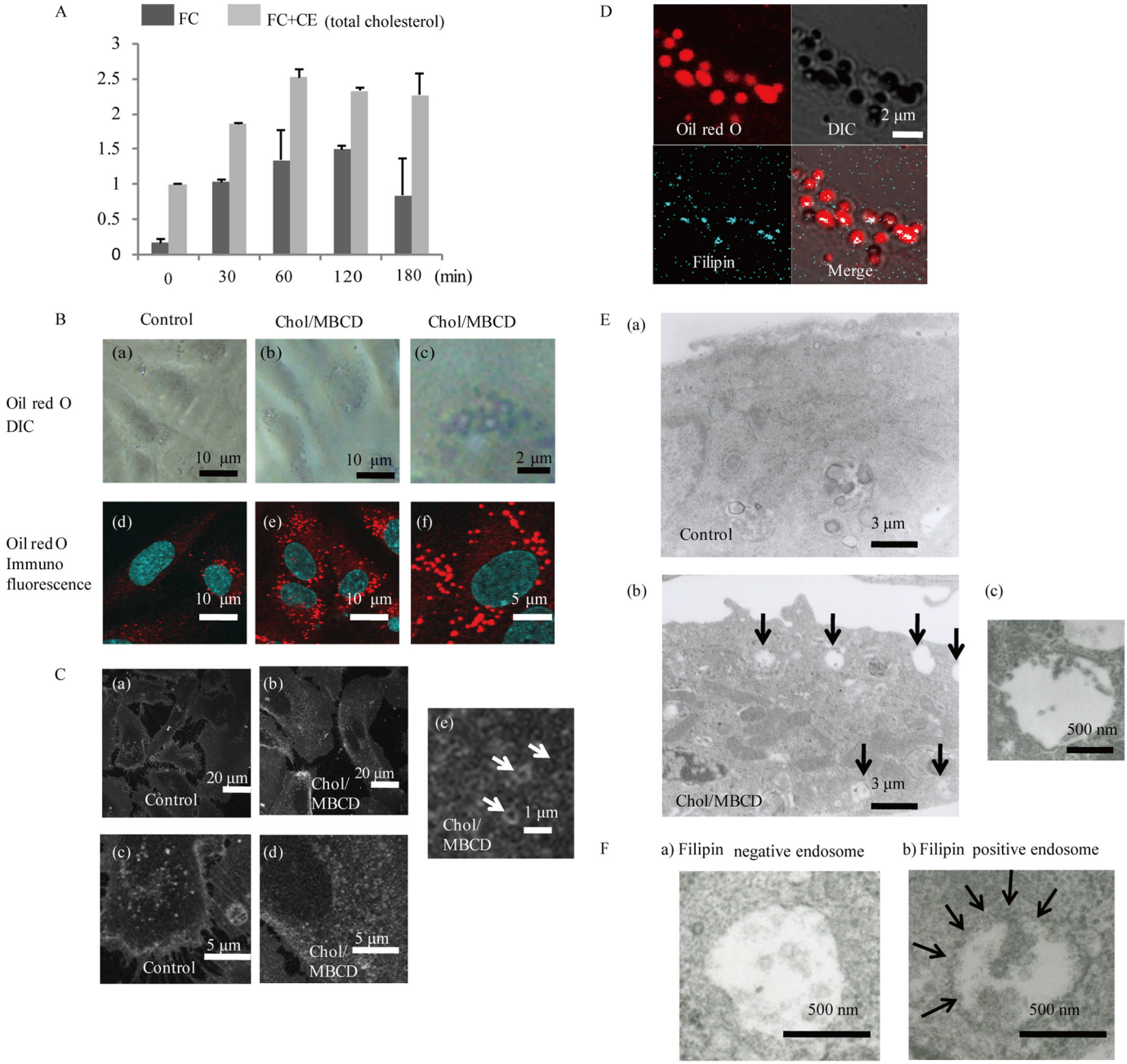

FIGURE 1. *A*, FC and total cholesterol (*FC+CE*) content at various times after Chol/MBCD loading. The data are represented as fold increase over intracellular total cholesterol concentration before Chol/MBCD incubation and are expressed as the means ± S.D. ($n = 3$). *FC*, free cholesterol; *CE*, cholesterol ester. *B*, visualization of vesicle structures using Oil Red O after Chol/MBCD loading. After Chol/MBCD loading (60 min), the cells were fixed and labeled with Oil Red O and observed with differential interference contrast (*DIC*) microscopy (*panels a–c*) and fluorescence confocal microscopy (*panels d–f*) using a Texas Red filter. *Panels c* and *f* are magnified images of *panels b* and *e*, respectively. *C*, FC localization using filipin staining in control conditions (*panels a* and *c*) and 60 min after Chol/MBCD loading (*panels b*, *d*, and *e*). *Panel e* is a magnified image of *panel d*, clearly showing the vesicle structures. *D*, co-staining with Oil Red O (*red*) and filipin (*blue*) 60 min after Chol/MBCD loading. *E*, *panel a*, electron microscopic images of HAECs under the preloading condition. Multivesicular bodies were rarely observed in control conditions. *Panel b*, electron microscopic images of HAECs 60 min after Chol/MBCD loading. Multivesicular bodies (*arrows*) are markedly increased and commonly observed in the cytoplasm. *Panel c*, magnified view of multivesicular body observed in *panel b*. *F*, electron microscopic images of multivesicular bodies observed under the Chol/MBCD loading condition using filipin staining. The cells were fixed 60 min after loading of Chol/MBCD. After fixation, they were labeled with filipin for 30 min. Filipin staining modified the outer and intraluminal membranes of some multivesicular bodies (filipin-positive endosome, *panel b*) to a wavy form compared with filipin-negative endosomes (*panel a*), suggesting the presence of FC.

vesicular bodies to a wavy form (Fig. 1*F*), suggesting the existence of FC within the membrane structures. These findings indicate that Chol/MBCD loading leads to the uptake of FC into cells and the formation of vesicle structures composed of FC-rich membranes, which correspond to the multivesicular bodies observed under electron microscopy, which are a type of late endosomes. Many similar multivesicular bodies were observed in ECs in atherosclerotic lesions of apolipoprotein E knock-out mice fed a Western diet for 15 weeks (supplemental Fig. S2), suggesting that the vesicle structures observed in cultured

HAECs could be detected in ECs *in vivo* under atherosclerotic conditions.

Intracellular FC-rich Membrane Microdomains—Next, we analyzed the relationship between the encapsulating membrane of the vesicles generated by FC enrichment and FC-rich membrane microdomains. We performed density gradient centrifugation to separate the FC-rich domains of the vesicle structures. Cell extracts were fractionated by density gradient centrifugation after treatment with 1% Triton X-100 and divided into nine fractions. The FC content in fractions 8 and 9 was extremely high and was considerably increased after Chol/MBCD loading, suggesting that these fractions contained FC-rich membrane domains of the vesicle structures generated by Chol/MBCD loading (Fig. 2*A*, *panels a–d*). Indeed, fractions 6–9 of Chol/MBCD loading samples contained Nile red-stained membrane structures, suggesting that the cytoplasmic vesicle structures induced by Chol/MBCD loading were of low density (supplemental Fig. S3). In preload conditions, most cellular proteins were present in fractions 1–4, as evidenced by the distribution of actin. Raft proteins such as Cav-1, Cav-2, and P-Cav-1, which were associated with FC-rich membrane domains, localized within fractions 5–7 (Fig. 2*B*). After Chol/MBCD loading, the locations of these raft proteins, particularly P-Cav-1, shifted to fractions 8 and 9, suggesting that these raft proteins were recruited to the newly formed FC-rich domain of the vesicle structures. In fraction 8 and 9, only FC increased, whereas cholesterol ester remained unchanged, suggesting that the association between FC and proteins identified in fraction 8 and 9 (Fig. 2*A*, *panel d*). Small GTPase Rac, which was present in fractions 1–4 in preload conditions, also shifted to fractions 8 and 9 after Chol/MBCD loading, suggesting an interaction with FC-rich membrane microdomains. Next, to confirm the shift of raft proteins toward the vesicle outer membranes, we performed immunohistochemistry of P-Cav-1, which was most clearly translocated toward fractions 8 and 9. In preload conditions, P-Cav-1 was found only in the PM fraction (Fig. 2*C*, *panel a*). After Chol/MBCD loading, P-Cav-1 was internalized into the cytoplasm and accumulated in the outer vesicle membrane (Fig. 2, *C*, *panels b–d*, and *D*), corresponding to the translocation of P-Cav-1 to fractions 8 and 9 in the fractionation experiment. This suggested that the shift to fractions 8 and 9 corresponded to the translocation to the outer membrane domains of the vesicle structures in the immunohistochemistry observations. Rac, Cav-1, and Cav-2 also accumulated in these membrane domains, as observed by immunohistochemical staining and image correlation analysis (Fig. 2*D* and supplemental Fig. S4).

Ang II Impaired eNOS Bioavailability in FC-enriched Conditions—Ang II is one of the pivotal factors affecting endothelial function as a donor of ROS, and its ROS production is closely associated with lipid raft microdomains (13, 25, 26). First, we checked the effect of modification of the FC condition on Ang II-induced ROS production (Fig. 3*A*). FC enrichment using Chol/MBCD loading alone did not affect the production of ROS, whereas it enhanced Ang II-induced ROS production. Next, we studied the effect of Ang II-induced ROS on endothelial function in the presence of vesicle structures (27). The basal phosphorylation state of eNOS is considered to be a surrogate marker of endothelial function; thus, we examined eNOS phosphorylation (Ser-1177) as a guide to study the effect of the presence of vesicle structures on endothelial function in HAECs (28). Chol/MBCD loading alone did not affect the level of eNOS phosphorylation markedly (data not shown). Ang II, which led to an increase in ROS production, had a minor impact on Ser-1177 eNOS phosphorylation and NO production (Fig. 3, *B*, *panel a*, and C). In contrast, Ang II markedly decreased eNOS phosphorylation compared with the base-line level in the FC-enriched condition (Fig. 3*B*, *panels b* and *c*), leading to a reduction in NO production (Fig. 3*C*). Subcellular localization of eNOS has a profound effect on its activity (29). Therefore, we investigated the modification of eNOS localization. In density fractionation studies, Chol/MBCD alone did not affect the position of eNOS in the gradient (Fig. 3*D*). The addition of Ang II shifted eNOS toward more detergent-resistant compartments, fractions 5–7, where Cav-1 and Cav-2 were enriched (supplemental Fig. S5). This shift was suppressed by MBCD pretreatment, suggesting that the shift was dependent on FC richness of these caveolin-rich membrane compartments. In contrast, co-treatment with Chol/MBCD and Ang II resulted in a marked shift of eNOS from lower density fractions to fractions 8 and 9. In fact, the eNOS in fractions 8 and 9 was not phosphorylated and was entirely composed of monomers (Fig. 3*E*), suggesting that the eNOS in fractions 8 and 9 is an inactive form. Furthermore, Hsp90, a critical co-factor in eNOS activation, did not exist in fractions 8 and 9 (data not shown). The translocation of eNOS toward fractions 8 and 9 is therefore associated with impairment of eNOS phosphorylation. The translocation of eNOS to fractions 8 and 9 was completely blocked by olmesartan or PD123319 (angiotensin receptor type I and type II blockers, respectively) and partially by DPI, apocynin, or *N*-acetylcysteine (Fig. 3*D*). These agents rescued eNOS phosphorylation (Fig. 3*F*), suggesting that the translocation of eNOS is dependent on Ang II receptor pathways and, at least partly, on ROS production. These results indicate that eNOS translocation is associated with the impairment of eNOS bioavailability, and this translocation is closely regulated by ROS production induced by Ang II.

Ang II-induced ROS Shifted eNOS toward Perinuclear Vesicles with FC-rich Membrane Microdomains—We confirmed these results by immunohistochemical studies. First, immunohistochemical studies of eNOS showed that Ang II shifted eNOS toward plasma membrane under the normal cholesterol condition, and this shift was seen to correspond to fractions 5–7 in fractionation (Fig. 4*A*, *panels a*, *b*, *e*, and *f*). On the other hand, under the FC-enriched condition, eNOS accumulated in the vesicle structures after Ang II stimulation (Fig. 4*A*, *panels c*, *d*, *g*, and *h*). Oil Red O staining revealed that vesicle structures were distributed diffusely in the cytoplasm under the preload condition (Fig. 4*B*, *panel a*), whereas the addition of Ang II resulted in shifting of the vesicles toward the perinuclear area (Fig. 4*B*, *panel b*). Next, we investigated the association between eNOS vesicle structures and Oil Red O-visualized vesicles. Co-staining with Oil Red O and eNOS showed the co-assembly of the vesicle structures and eNOS in the perinuclear area, in contrast to the results obtained with Chol/MBCD incubation alone (Fig. 4*C*).

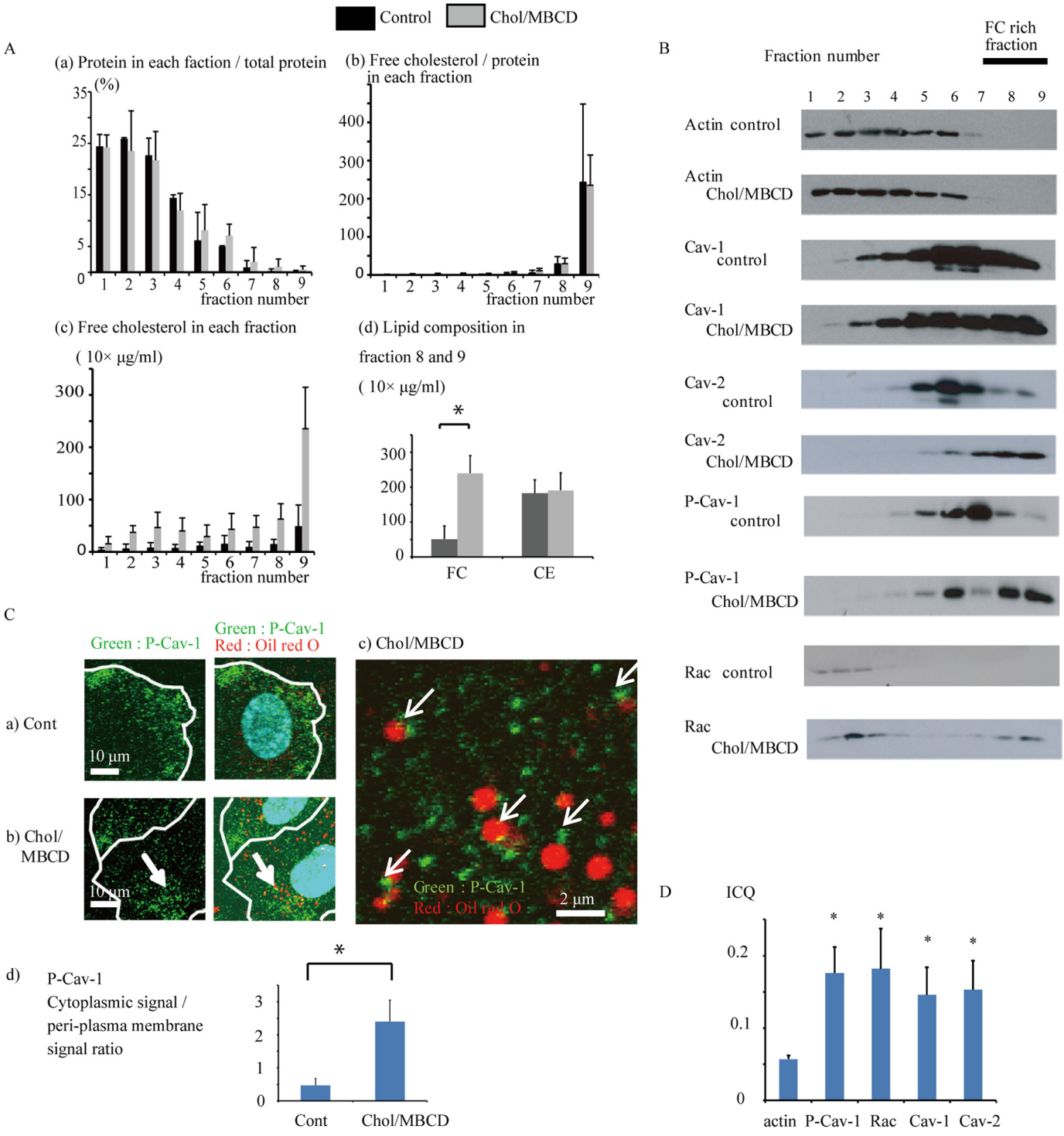

FIGURE 2. *A*, *panel a*, distribution of proteins in control conditions and after Chol/MBCD incubation for 1 h after density gradient centrifugation. The amount of protein in each fraction is expressed as a percentage of that found in total fractions ($n = 3$). Most cellular proteins were recovered in fractions 1–5, whereas Chol/MBCD treatment shifted the protein distribution to the more detergent-resistant fractions. *Panel b*, FC/protein ratio in each fraction after density gradient centrifugation. The figure shows the distribution of FC after correction for protein content in each fraction ($n = 3$). FC content in fractions 8 and 9 was extremely high; thus, the FC-enriched membrane fractions were segregated into these fractions. *Panel c*, absolute value of FC content in each fraction after density gradient centrifugation ($n = 3$). The absolute FC content mainly increased in fractions 8 and 9 after Chol/MBCD treatment; therefore, these fractions contained proteins that existed within the membrane domain associated with exogenously loaded FC. *Panel d*, lipid composition in fractions 8 and 9 in control conditions and after Chol/MBCD treatment for 1 h ($n = 3$). *, $p < 0.05$. *B*, representative immunoblotting signals demonstrating distribution of key proteins in preloading conditions and 60 min after Chol/MBCD loading in density gradient fractions ($n = 3$). Cell extracts were subjected to density gradient centrifugation and then divided into nine fractions and analyzed by Western blotting, using specific antibodies against actin, Cav-1, Cav-2, P-Cav-1 (Tyr-14), and Rac. *C*, co-staining with Oil Red O (*red*) and P-Cav-1 (*green*) in control conditions (*panel a*) and 60 min after Chol/MBCD loading (*panel b*). *Panel c*, is a magnified image of *panel b*. The edge of the cell is outlined in *white*. *Panel d*, quantitative analysis of P-Cav-1 cytoplasmic signal/peri-plasma membrane signal ratio of HAECs in control conditions and after Chol/MBCD loading (60 min). P-Cav-1 signal intensities of 5 μm in cytoplasm and plasma membrane were averaged ($n = 5$). *, $p < 0.05$. *D*, ICQ analysis of co-localization of actin, P-Cav-1, Rac, Cav-1, and Cav-2 with Oil Red O vesicles ($n = 5$). The results are presented as the means ± S.D. ($n = 5$). *, $p < 0.05$ *versus* ICQ of actin that was co-localized with Oil Red O. *Cont*, control.

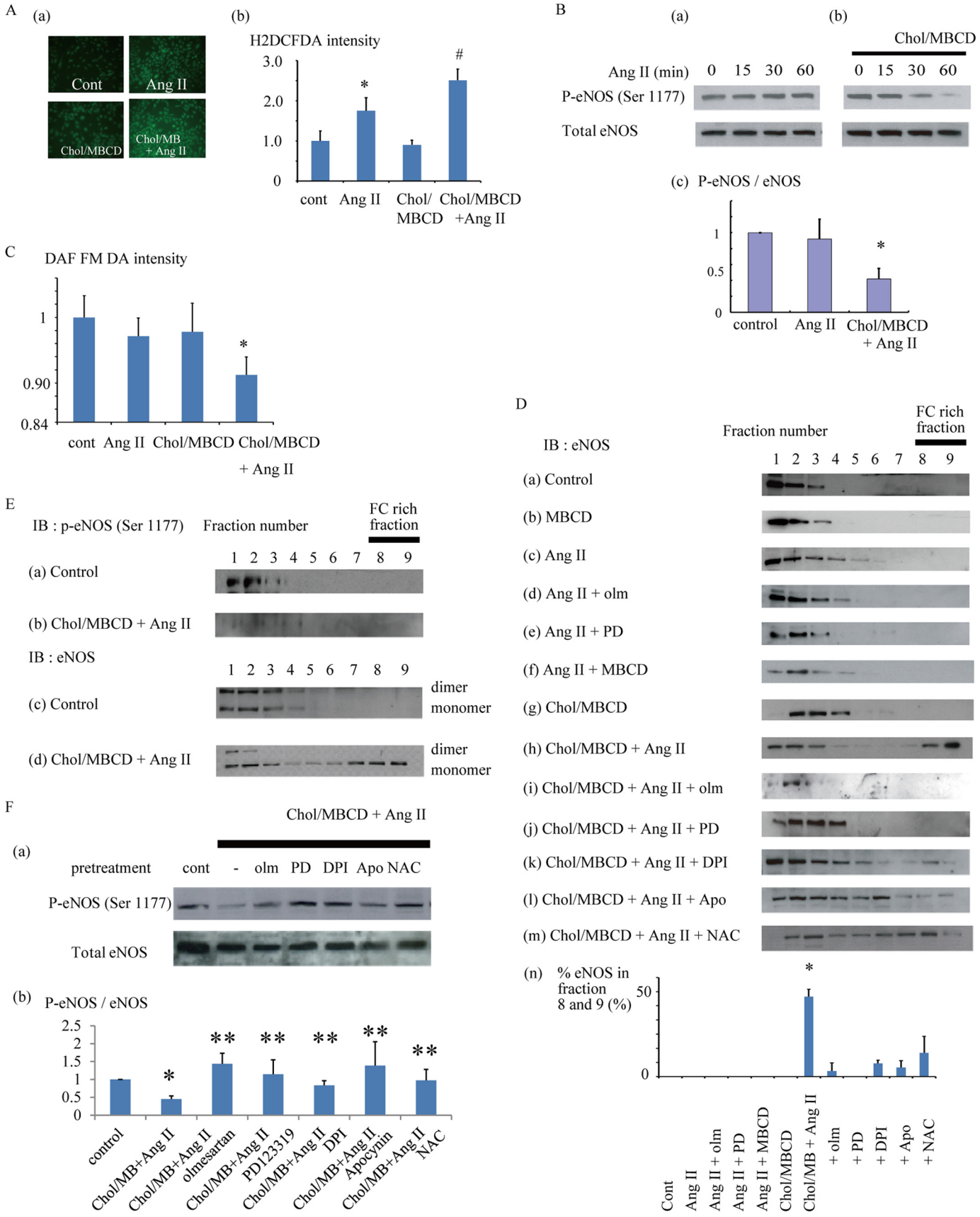
A
(a)
Cont
Ang II
Chol/MBCD
Chol/MB + Ang II
(b)
H2DCFDA intensity
3.0
2.0
1.0
0
cont
Ang II
Chol/ MBCD
Chol/MBCD +Ang II
B
(a)
(b)
Chol/MBCD
Ang II (min) 0 15 30 60
0 15 30 60
P-eNOS (Ser 1177)
Total eNOS
(c) P-eNOS / eNOS
1
0.5
0
control
Ang II
Chol/MBCD + Ang II
C
DAF FM DA intensity
1
0.90
0.84
cont
Ang II
Chol/MBCD
Chol/MBCD + Ang II
D
Fraction number
FC rich fraction
IB : eNOS
1 2 3 4 5 6 7 8 9
(a) Control
(b) MBCD
(c) Ang II
(d) Ang II + olm
(e) Ang II + PD
(f) Ang II + MBCD
(g) Chol/MBCD
(h) Chol/MBCD + Ang II
(i) Chol/MBCD + Ang II + olm
(j) Chol/MBCD + Ang II + PD
(k) Chol/MBCD + Ang II + DPI
(l) Chol/MBCD + Ang II + Apo
(m) Chol/MBCD + Ang II + NAC
(n) % eNOS in fraction 8 and 9 (%)
50
0
Cont
Ang II
Ang II + olm
Ang II + PD
Ang II + MBCD
Chol/MBCD
Chol/MB + Ang II
+ olm
+ PD
+ DPI
+ Apo
+ NAC
E
IB : p-eNOS (Ser 1177)
Fraction number
FC rich fraction
1 2 3 4 5 6 7 8 9
(a) Control
(b) Chol/MBCD + Ang II
IB : eNOS
(c) Control
(d) Chol/MBCD + Ang II
dimer
monomer
F
Chol/MBCD + Ang II
(a)
pretreatment cont - olm PD DPI Apo NAC
P-eNOS (Ser 1177)
Total eNOS
(b) P-eNOS / eNOS
2.5
2
1.5
1
0.5
0
control
Chol/MB+Ang II
olmesartan
PD123319
DPI
Apocynin
NAC

Because the perinuclear vesicles are thought to be associated with perinuclear organelles, we investigated the localization of several organelle markers in association with vesicles. Fractionation experiments showed that Rab7, a late endosome marker, was increased under the Chol/MBCD loading condition (Fig. 5*A*, *panel a*) and LAMP-1, a late endosome/lysosome marker, was increased after Chol/MBCD with Ang II loading in fractions 8 and 9 of the density gradient (Fig. 5*A*, *panel b*). On the other hand, EEA-1 and golgin-97, early endosome marker and Golgi marker, did not change position in the fractions (Fig. 5*A*, *panels c* and *d*). An intensity correlation analysis of co-localization of Oil Red O and Rab7 or LAMP-1 revealed a significant increase in ICQ score, suggesting a close association between the vesicles and Rab7 under the Chol/MBCD loading condition (Fig. 5*B* and supplemental Fig. S6, *panels a* and *e*) or between the vesicles and LAMP-1-labeled endosomes under the Ang II with and without Chol/MBCD condition (Fig. 5*B* and supplemental Fig. S6, *panels* b and *f*), compared with EEA-1 or golgin-97 (Fig. 5*B* and supplemental Fig. S6, *panels c* and *d*). The shifting of Rab7 and LAMP-1 to fractions 8 and 9 in the density fractionation experiment was compatible with co-localization of the vesicles and late endosome/lysosome organelles. These results suggested that vesicles induced by FC enrichment initially had a close association with Rab7-labeled endosomes, that Ang II shifted these vesicles toward the perinuclear area, and that these vesicles were closely associated with LAMP-1-labeled endosomes. Indeed, not only Oil Red O vesicles but vesicles visualized by filipin were also co-localized with LAMP-1 in the perinuclear area on Ang II stimulation (supplemental Fig. S7). In addition, electron microscopy revealed an increase in electron-dense lysosomal structures (0.5–1 μm in size) that contained FC-rich membrane compartments around the nucleus (Fig. 5*C*). Also, as seen with vesicles in immunohistochemical studies, Ang II treatment led to the accumulation of P-Cav-1 within the LAMP-1-labeled endosomes in the perinuclear area (Fig. 5*D*). These proteins also shifted toward fractions 8 and 9 in density fractionation experiments (Fig. 2*B*). Therefore, it was evident that intracellular FC-rich membrane microdomains also translocated toward the perinuclear late endosomes/lysosomes together with the vesicle structures.

According to the relationship between eNOS and cytoplasmic organelles, LAMP-1-labeled endosomes were also co-localized with eNOS in the perinuclear area (Fig. 5*E*, *panels a* and *b*), and this translocation of eNOS toward LAMP-1 was suppressed by olmesartan or ROS inhibitors (Fig. 5*E*, *panels c–e*). The results of density fractionation and immunohistochemical studies suggested that under the FC-enriched condition, Ang II induces eNOS assembly around the vesicle membrane, leading to a close association of these compartments with the late endosomes/lysosomes in the perinuclear area and impairment of eNOS function. This eNOS trafficking is dependent on Ang II-induced ROS production.

DISCUSSION

In the present study, we found that vesicle structures composed of an FC-enriched membrane were formed in HAECs under FC-loading conditions. The vesicle structures functioned as an intracellular platform of signal transduction. In addition, Ang II induced perinuclear assembly of the vesicles in which eNOS was trapped, thus reducing eNOS bioavailability.

Several reports have demonstrated that vesicles rich in FC can be isolated from atherosclerotic tissues (30, 31). These vesicles were thought to be an early pathological form of accumulated cholesterol in developing atherosclerotic lesions and appeared to be derived from the degradation product of plasma LDL. However, these vesicles were clearly distinct from LDL particles. In addition, they could be taken up or transcytosed by ECs. Indeed, ECs in atherosclerotic lesions of cholesterol-fed animals were reported to contain similar vesicles (12, 32).

In this study, the outer membranes of the vesicle structures showed characteristics similar to those of lipid rafts. Many intracellular organelles appear to contain raft-like domains in addition to the PM (33, 34). In particular, intracellular Cav-1-containing vesicle structures are one example of vesicle structures that have characteristics similar to those of lipid raft

FIGURE 3. *A*, mean fluorescent intensities of H2DCFDA indicative of intracellular ROS production after Ang II stimulation (200 nmol/liter) with or without Chol/MBCD loading and Chol/MBCD loading alone in HAECs. Fluorescence microscopic findings in each condition are presented (*panel a*). The data are represented as fold increases over mean fluorescent intensity in the preload condition ($n = 5$). *, $p < 0.05$ *versus* control; #, $p < 0.05$ *versus* Ang II (*panel b*). *B*, Western blotting of p-eNOS (Ser-1177) after Ang II stimulation (200 nmol/liter) with (*panel b*) or without (*panel a*) Chol/MBCD loading. Cells were extracted at the indicated times after Ang II stimulation. Chol/MBCD loading was performed 30 min before Ang II stimulation. *Panel c*, relative quantitation of p-eNOS (Ser-1177)/eNOS 60 min after Ang II stimulation with or without Chol/MBCD. The data are presented as fold increases over control conditions ($n = 7$; analysis of variance). *, $p < 0.0001$. *C*, mean fluorescent intensities of DAF-FM DA indicative of NO production after Ang II stimulation (200 nmol/liter) with or without Chol/MBCD loading in HAECs. The data are presented as fold increases over mean fluorescent intensity in the preload condition. ($n = 5$; analysis of variance). *, $p < 0.01$. *D*, distribution of eNOS protein in density fractions. The cells were extracted in control conditions (*panel a*), MBCD loading (2 mmol/liter, 30 min) (*panel b*), after Ang II stimulation (200 nmol/liter, 30 min) (*panel c*), with olmesartan (4 μmol/liter) (*panel d*), PD123319 (10 μmol/liter) (*panel e*), MBCD (2 mmol/liter) (*panel f*), or Chol/MBCD loading (60 min; Chol/MBCD loading was performed 30 min before Ang II stimulation) (*panel h*) and after Chol/MBCD loading alone (60 min) (*panel g*). Olmesartan, PD123319, and MBCD were loaded 15 min before Ang II treatment. Ang II treatment after pretreatment with olmesartan (4 μmol/liter) (*panel i*), PD123319 (10 μmol/liter) (*panel j*), DPI (0.5 μmol/liter) (*panel k*), apocynin (8 μmol/liter) (*panel l*), or *N*-acetylcysteine (*NAC*, 80 μmol/liter) (*panel m*) was also performed 15 min after Chol/MBCD loading. *Panel n*, percentage of eNOS protein distribution in fractions 8 and 9 combined after density fractionation. The relative quantitative value of eNOS in each fraction was determined by densitometry, and the percentage of eNOS in fractions 8 and 9 was calculated. Each bar in the graphs represents the mean ± S.D. of three independent experiments. *, $p < 0.05$. *E*, localization of p-eNOS (Ser-1177) protein in density fractions. We examined the phosphorylation of eNOS (Ser-1177) in each fraction in control conditions (*panel a*) and after Ang II stimulation (200 nmol/liter, 30 min) with Chol/MBCD loading (60 min) (*panel b*). Coupling status of eNOS in density fractions in control conditions (*panel c*) and after Ang II stimulation (200 nmol/liter, 30 min) with Chol/MBCD loading (60 min) (*panel d*). eNOS dimers and monomers were separated by low temperature SDS-PAGE. *F*, *panel a*, Western blotting of p-eNOS (Ser-1177) with pretreatment by Ang II receptor blockers or ROS inhibitors. After Chol/MBCD loading, pretreatment with olmesartan (4 μmol/liter), PD123319 (10 μmol/liter), DPI (0.5 μmol/liter), apocynin (8 μmol/liter), or *N*-acetylcysteine (80 μmol/liter) was performed. Next, Ang II (200 nmol/liter, 30 min) was administered, and the cells were extracted. *Panel b*, the relative quantitative value of p-eNOS/eNOS is presented as fold increase over control conditions ($n = 3$). *, significantly different from control ($p < 0.05$); **, significantly different from Ang II with Chol/MBCD ($p < 0.05$). *Cont* or *cont*, control; *IB*, immunoblot; *olm*, olmesartan.

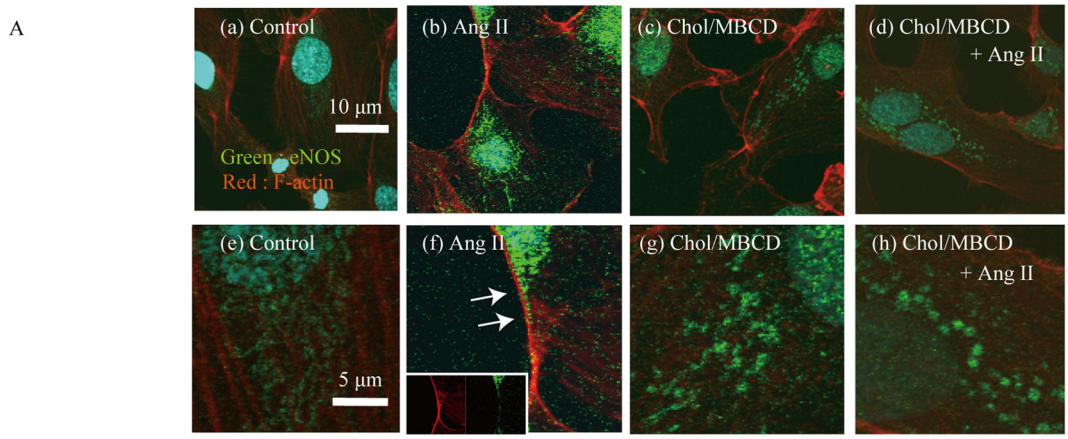

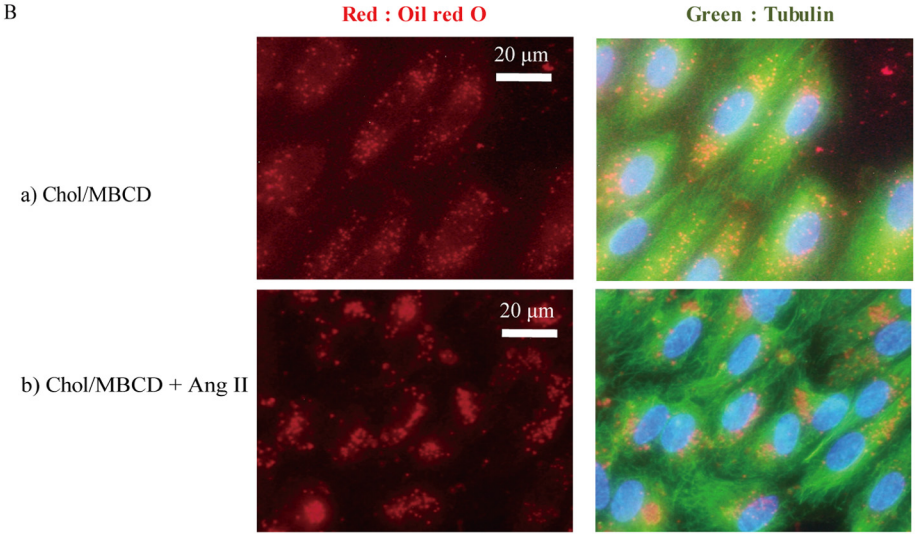

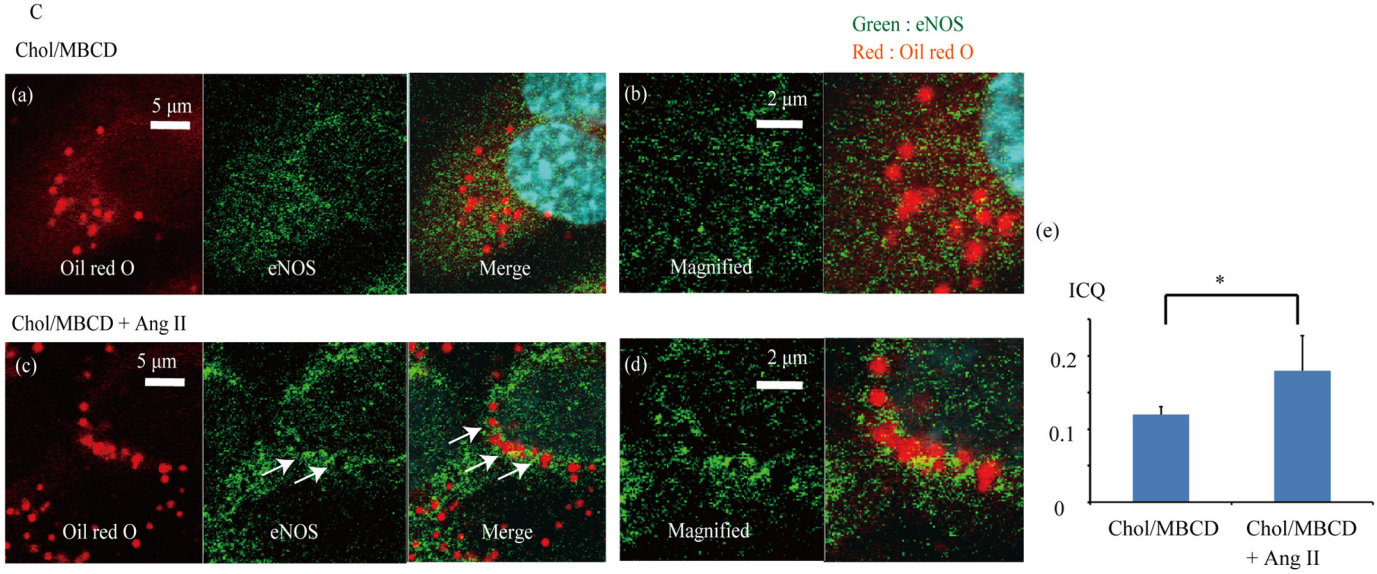

FIGURE 4. *A*, immunohistochemical staining of eNOS in control conditions (*panels a* and *e*), with Chol/MBCD loading (60 min) (*panels c* and *g*), and with Ang II stimulation (200 nmol/liter, 30 min) with (*panels d* and *h*) and without (*panels b* and *f*) Chol/MBCD loading (60 min). Chol/MBCD loading was performed 30 min before Ang II stimulation. Co-immunostaining of eNOS (*green*) and F-actin (*red*) was performed. *Panels e–h* are magnified images of *panels a–d*, respectively. *B*, *panels a* and *b*, co-staining with Oil Red O (*red*) and anti-tubulin antibody (*green*) 60 min after Chol/MBCD loading (*panel a*) and Chol/MBCD loading with Ang II (200 nmol/liter, 30 min) (*panel b*). Chol/MBCD loading was performed 30 min before Ang II stimulation. *C*, co-staining with Oil Red O (*red*) and eNOS antibody (*green*) with (*panels c* and *d*) or without (*panel a* and *b*) Ang II (200 nmol/liter, 30 min) after Chol/MBCD loading. Chol/MBCD loading was performed 30 min before Ang II stimulation. *Panel e*, ICQ analysis of co-localization between eNOS and Oil Red O vesicles with or without Ang II (200 nmol/liter, 30 min) after Chol/MBCD loading ($n = 5$). The results are presented as the means ± S.D. *, $p < 0.05$.

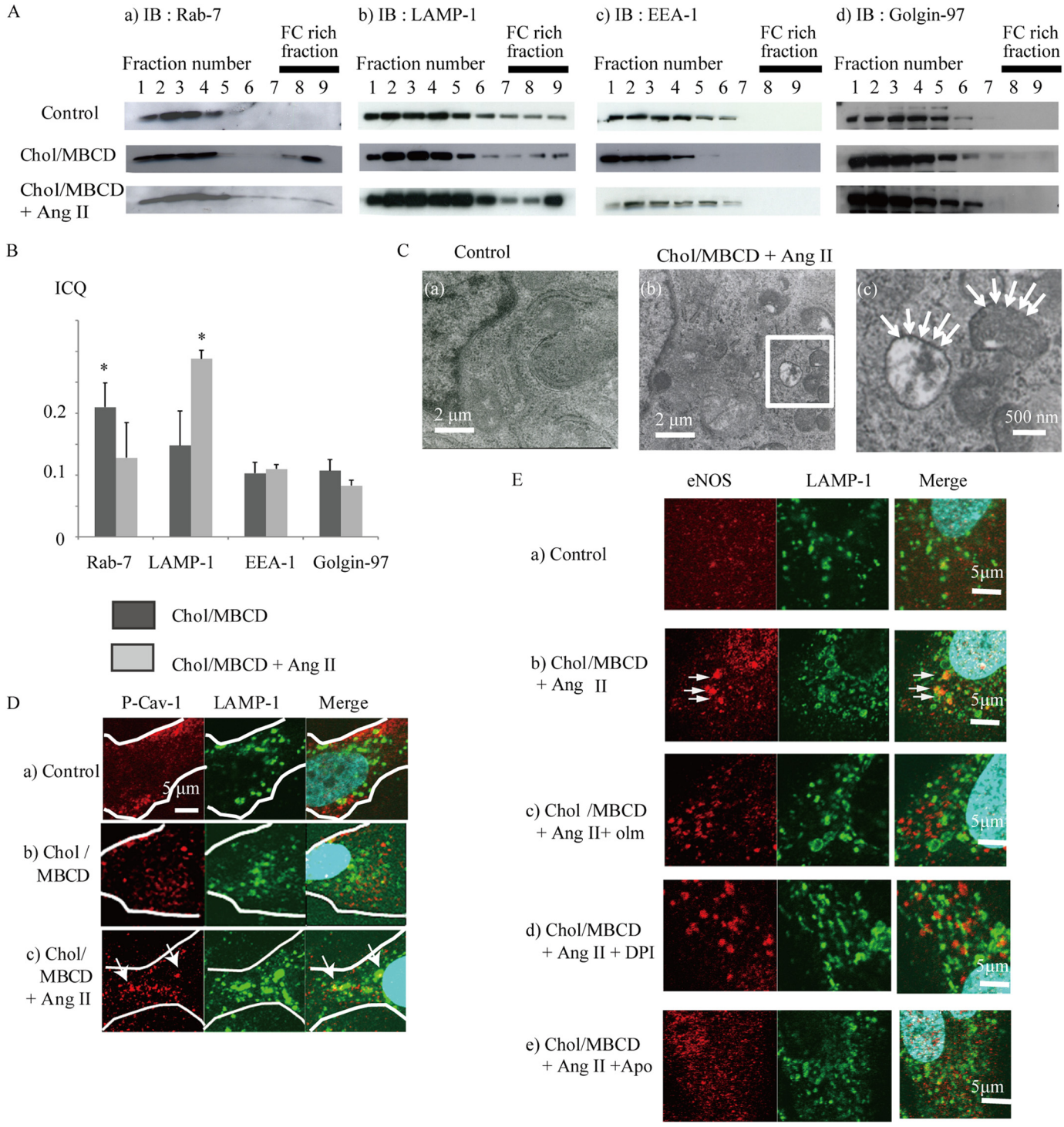

FIGURE 5. *A*, subcellular localization of Rab7 (*panel a*), LAMP-1 (*panel b*), EEA-1 (*panel c*), and golgin-97 (*panel d*) protein in density gradient fractions 60 min after Chol/MBCD incubation with or without addition of Ang II (200 nmol/liter, 30 min). Chol/MBCD loading was performed 30 min before Ang II stimulation. *B*, ICQ analysis of co-localization between Oil Red O vesicles and each endosome marker protein (Rab7, LAMP-1, EEA-1, and golgin-97) in Chol/MBCD loading (60 min) and Chol/MBCD loading plus Ang II (200 nmol/liter, 30 min) conditions. The images of co-staining of Oil Red O and each endosome marker proteins were presented in supplemental Fig. S6. Chol/MBCD loading was performed 30 min before Ang II stimulation. The results are presented as the means ± S.D. *, $p < 0.05$ *versus* ICQ of EEA-1 and Golgin-97. *C*, filipin staining of lysosomal compartments observed in control conditions (*panel a*) and after Ang II stimulation (200 nmol/liter, 30 min) with Chol/MBCD loading (60 min) (*panels b* and *c*) by electron microscopy. In addition to the outer membrane of multivesicular bodies, the outer membranes of lysosomal structures were also modified by filipin to a wavy form (*arrows*). *D*, co-immunostaining with P-Cav-1 (*red*) and LAMP-1 (*green*) in control conditions (*panel a*), with Chol/MBCD loading (60 min) (*panel b*) and with Chol/MBCD loading (60 min) plus Ang II stimulation (200 nmol/liter, 30 min) (*panel c*). Chol/MBCD loading was performed 30 min before Ang II stimulation. The edge of the cell is outlined in *white*. *E*, co-immunostaining with LAMP-1 (*green*) and eNOS (*red*) in olmesartan or ROS inhibitor pretreatment condition. Ang II (200 nmol/liter, 30 min) and Chol/MBCD (60 min) were added alone (*panel b*) or in the presence of olmesartan (4 μmol/liter) (*panel c*), DPI (0.5 μmol/liter) (*panel d*), or apocynin (8 μmol/liter) (*panel e*). *Panel a* shows the control conditions. The cells were fixed and stained. Olmesartan pretreatment markedly suppressed eNOS translocation toward LAMP-1-labeled endosomes. The co-localized signal is indicated in *yellow*. *Apo*, apocynin; *IB*, immunoblot; *olm*, olmesartan.

microdomains and that are reported to have a critical role in the transport of some proteins and lipids (35). However, the function of this intracellular raft-like domain as a signal transduction platform in ECs had not been elucidated previously. In this study, we demonstrated that the intracellular FC-rich membrane microdomain has an important role in regulating eNOS function.

In this study, the effect of Ang II on eNOS activation was regulated by cellular cholesterol conditions. Ang II was reported to induce NO production by eNOS shift to membrane raft compartments (16, 35). However, NO produced by Ang II was quenched by simultaneously produced reactive oxygen produced by NADPH oxidase, resulting in peroxynitrite formation. The balance between the two pathways was regulated in a caveolin-dependent manner (16). We also verified the effect of Ang II on eNOS translocation and NO production, because Ang II with the ROS inhibitor DPI led to considerable NO production (data not shown). In HAECs, this Ang II-induced translocation had a minor impact on eNOS phosphorylation and net NO production in the normal cholesterol environment. On the other hand, FC enrichment considerably modified this Ang II-induced response. FC enrichment generated intracellular FC-rich membrane microdomains and shifted the site to which eNOS was targeted by Ang II, resulting in eNOS accumulation toward the perinuclear lysosomes and marked reduction in eNOS Ser-1177 phosphorylation and NO production. The effect of Ang II on eNOS was modified by changing its localization in a cellular cholesterol-dependent manner.

The reason for eNOS Ser-1177 phosphorylation being markedly suppressed is presumed to be related to the translocation of eNOS and the characteristics of its compartments, such as the absence of Hsp90 (36, 37). The absence of binding to Hsp90 of eNOS in this compartment was confirmed by the inability of eNOS to form a dimer. Alternatively, the ROS produced, such as peroxynitrite, may be associated with eNOS inactivation (38–40). In addition, lysosomal targeting also modified the activity and expression of some proteins (41, 42). These mechanisms may contribute to eNOS inactivation.

The mechanism of vesicle and FC-rich membrane microdomain compartment translocation toward the perinuclear area was presumed to be associated with ROS production. Indeed, the immunohistochemistry of eNOS showed that suppression of Ang II-induced ROS obstructed the movement of eNOS trafficking toward late endosomes and suppressed eNOS impairment by Ang II with Chol/MBCD. The association between the oxidation process and perinuclear translocation was studied before. Conrad *et al.* (41) demonstrated that cholesterol oxidase induced caveolin translocation between PM caveolae and the Golgi complex. Oxidized LDL-derived FC, but not that derived from other lipoproteins, accumulated in the perinuclear area (42, 43). There are also reports that trafficking patterns of PM proteins to lysosomes may be altered under oxidative stress (44, 45). These translocations were presumed to be affected by the oxidized state of constituent membrane lipids. Indeed, lipids within biological membranes are thought to be among the preferential targets of ROS that cause lipid oxidation, resulting in modification of membrane properties and functions. This lipid oxidation-derived effect may also change the transfer target of oxidized lipid-containing compartments.

These results also suggest that the presence of intracellular vesicle structures may be a phenotypic feature of dysfunction in ECs. Previous studies have reported that late endosomal lipid storage leads to endothelial dysfunction in lysosomal storage disease and in *Chlamydia* infection (46, 47). In addition, these abnormalities have been reported to be associated with an increase in ROS (48), suggesting that intracellular vesicles are a location for intracellular production of reactive oxygen.

In conclusion, this study demonstrated the biogenesis of vesicle structures after FC enrichment of HAECs that led to the modulation of signaling pathways. Ang II causes vesicle structures containing eNOS to fuse with endocytic pathways in the perinuclear area, resulting in eNOS dysfunction in an ROS-dependent manner. These findings provide a novel insight into the mechanisms of endothelial dysfunction in hypercholesterolemia.

Acknowledgments—We are grateful to Satoru Fukuda and Chie Fujinami for technical assistance.

REFERENCES

1. Cox, D. A., and Cohen, M. L. (1996) Effects of oxidized low-density lipoprotein on vascular contraction and relaxation. Clinical and pharmacological implications in atherosclerosis. *Pharmacol. Rev.* **48,** 3–19
2. Mehta, J. L., Sanada, N., Hu, C. P., Chen, J., Dandapat, A., Sugawara, F., Satoh, H., Inoue, K., Kawase, Y., Jishage, K., Suzuki, H., Takeya, M., Schnackenberg, L., Beger, R., Hermonat, P. L., Thomas, M., and Sawamura, T. (2007) Deletion of LOX-1 reduces atherogenesis in LDLR knockout mice fed high cholesterol diet. *Circ. Res.* **100,** 1634–1642
3. Simionescu, N., Vasile, E., Lupu, F., Popescu, G., and Simionescu, M. (1986) Prelesional events in atherogenesis. Accumulation of extracellular cholesterol-rich liposomes in the arterial intima and cardiac valves of the hyperlipidemic rabbit. *Am. J. Pathol.* **123,** 109–125
4. Grosheva, I., Haka, A. S., Qin, C., Pierini, L. M., and Maxfield, F. R. (2009) Aggregated LDL in contact with macrophages induces local increases in free cholesterol levels that regulate local actin polymerization. *Arterioscler. Thromb. Vasc. Biol.* **29,** 1615–1621
5. Hakala, J. K., Oksjoki, R., Laine, P., Du, H., Grabowski, G. A., Kovanen, P. T., and Pentikäinen, M. O. (2003) Lysosomal enzymes are released from cultured human macrophages, hydrolyze LDL in vitro, and are present extracellularly in human atherosclerotic lesions. *Arterioscler. Thromb. Vasc. Biol.* **23,** 1430–1436
6. Qin, C., Nagao, T., Grosheva, I., Maxfield, F. R., and Pierini, L. M. (2006) Elevated plasma membrane cholesterol content alters macrophage signaling and function. *Arterioscler. Thromb. Vasc. Biol.* **26,** 372–378
7. Paragh, G., Kovács, E., Seres, I., Keresztes, T., Balogh, Z., Szabó, J., Teichmann, F., and Fóris, G. (1999) Altered signal pathway in granulocytes from patients with hypercholesterolemia. *J. Lipid Res.* **40,** 1728–1733
8. Fang, Y., Mohler, E. R., 3rd, Hsieh, E., Osman, H., Hashemi, S. M., Davies, P. F., Rothblat, G. H., Wilensky, R. L., and Levitan, I. (2006) Hypercholesterolemia suppresses inwardly rectifying K+ channels in aortic endothelium in vitro and in vivo. *Circ. Res.* **98,** 1064–1071
9. Feng, B., Yao, P. M., Li, Y., Devlin, C. M., Zhang, D., Harding, H. P., Sweeney, M., Rong, J. X., Kuriakose, G., Fisher, E. A., Marks, A. R., Ron,

D., and Tabas, I. (2003) The endoplasmic reticulum is the site of cholesterol-induced cytotoxicity in macrophages. *Nat. Cell Biol.* **5,** 781–792
10. Porto, A., Palumbo, R., Pieroni, M., Aprigliano, G., Chiesa, R., Sanvito, F., Maseri, A., and Bianchi, M. E. (2006) Smooth muscle cells in human atherosclerotic plaques secrete and proliferate in response to high mobility group box 1 protein. *FASEB J.* **20,** 2565–2566
11. Rong, J. X., Shapiro, M., Trogan, E., and Fisher, E. A. (2003) Transdifferentiation of mouse aortic smooth muscle cells to a macrophage-like state after cholesterol loading. *Proc. Natl. Acad. Sci. U.S.A.* **100,** 13531–13536
12. Kim, J. A., Maxwell, K., Hajjar, D. P., and Berliner, J. A. (1991) β-VLDL increases endothelial cell plasma membrane cholesterol. *J. Lipid Res.* **32,** 1125–1131
13. Yang, B., Oo, T. N., and Rizzo, V. (2006) Lipid rafts mediate H_2O_2 prosurvival effects in cultured endothelial cells. *FASEB J.* **20,** 1501–1503
14. Pritchard, K. A., Ackerman, A. W., Ou, J., Curtis, M., Smalley, D. M., Fontana, J. T., Stemerman, M. B., and Sessa, W. C. (2002) Native low-density lipoprotein induces endothelial nitric oxide synthase dysfunction. Role of heat shock protein 90 and caveolin-1. *Free Radic. Biol. Med.* **33,** 52–62
15. Morikage, N., Kishi, H., Sato, M., Guo, F., Shirao, S., Yano, T., Soma, M., Hamano, K., Esato, K., and Kobayashi, S. (2006) Cholesterol primes vascular smooth muscle to induce Ca2 sensitization mediated by a sphingosylphosphorylcholine-Rho-kinase pathway. Possible role for membrane raft. *Circ. Res.* **99,** 299–306
16. Jin, S., Zhang, Y., Yi, F., and Li, P. L. (2008) Critical role of lipid raft redox signaling platforms in endostatin-induced coronary endothelial dysfunction. *Arterioscler. Thromb. Vasc. Biol.* **28,** 485–490
17. Zhang, C., and Li, P. L. (2010) Membrane raft redox signalosomes in endothelial cells. *Free Radic. Res.* **44,** 831–842
18. Robinson, J. M., and Vandré, D. D. (2001) Antigen retrieval in cells and tissues. Enhancement with sodium dodecyl sulfate. *Histochem. Cell Biol.* **116,** 119–130
19. Li, Q., Lau, A., Morris, T. J., Guo, L., Fordyce, C. B., and Stanley, E. F. (2004) A syntaxin 1, $G\alpha_o$, and N-type calcium channel complex at a presynaptic nerve terminal. Analysis by quantitative immunocolocalization. *J. Neurosci.* **24,** 4070–4081
20. Zidovetzki, R., and Levitan, I. (2007) Use of cyclodextrins to manipulate plasma membrane cholesterol content. Evidence, misconceptions and control strategies. *Biochim. Biophys. Acta* **1768,** 1311–1324
21. Ravi, K., Brennan, L. A., Levic, S., Ross, P. A., and Black, S. M. (2004) *S*-Nitrosylation of endothelial nitric oxide synthase is associated with monomerization and decreased enzyme activity. *Proc. Natl. Acad. Sci. U.S.A.* **101,** 2619–2624
22. Terasaka, N., Yu, S., Yvan-Charvet, L., Wang, N., Mzhavia, N., Langlois, R., Pagler, T., Li, R., Welch, C. L., Goldberg, I. J., and Tall, A. R. (2008) ABCG1 and HDL protect against endothelial dysfunction in mice fed a high-cholesterol diet. *J. Clin. Invest.* **118,** 3701–3713
23. Koopman, R., Schaart, G., and Hesselink, M. K. (2001) Optimisation of Oil Red O staining permits combination with immunofluorescence and automated quantification of lipids. *Histochem. Cell Biol.* **116,** 63–68
24. McGookey, D. J., Fagerberg, K., and Anderson, R. G. (1983) Filipin-cholesterol complexes form in uncoated vesicle membrane derived from coated vesicles during receptor-mediated endocytosis of low density lipoprotein. *J. Cell Biol.* **96,** 1273–1278
25. Zuo, L., Ushio-Fukai, M., Ikeda, S., Hilenski, L., Patrushev, N., and Alexander, R. W. (2005) Caveolin-1 is essential for activation of Rac1 and NAD(P)H oxidase after angiotensin II type 1 receptor stimulation in vascular smooth muscle cells. Role in redox signaling and vascular hypertrophy. *Arterioscler. Thromb. Vasc. Biol.* **25,** 1824–1830
26. Lobysheva, I., Rath, G., Sekkali, B., Bouzin, C., Feron, O., Gallez, B., Dessy, C., and Balligand, J. L. (2011) Moderate caveolin-1 downregulation prevents NADPH oxidase-dependent endothelial nitric oxide synthase uncoupling by angiotensin II in endothelial cells. *Arterioscler. Thromb. Vasc. Biol.* **31,** 2098–2105
27. Landmesser, U., Hornig, B., and Drexler, H. (2004) Endothelial function. A critical determinant in atherosclerosis? *Circulation* **109,** II27–33
28. Du, X. L., Edelstein, D., Dimmeler, S., Ju, Q., Sui, C., and Brownlee, M. (2001) Hyperglycemia inhibits endothelial nitric oxide synthase activity by posttranslational modification at the Akt site. *J. Clin. Invest.* **108,** 1341–1348
29. Sánchez, F. A., Rana, R., Kim, D. D., Iwahashi, T., Zheng, R., Lal, B. K., Gordon, D. M., Meininger, C. J., and Durán, W. N. (2009) Internalization of eNOS and NO delivery to subcellular targets determine agonist-induced hyperpermeability. *Proc. Natl. Acad. Sci. U.S.A.* **106,** 6849–6853
30. Kruth, H. S. (1984) Histochemical detection of esterified cholesterol within human atherosclerotic lesions using the fluorescent probe filipin. *Atherosclerosis* **51,** 281–292
31. Chao, F. F., Amende, L. M., Blanchette-Mackie, E. J., Skarlatos, S. I., Gamble, W., Resau, J. H., Mergner, W. T., and Kruth, H. S. (1988) Unesterified cholesterol-rich lipid particles in atherosclerotic lesions of human and rabbit aortas. *Am. J. Pathol.* **131,** 73–83
32. Simionescu, M., Stancu, C., Costache, G., and Sima, A. (2002) Endothelial cell response to hyperlipemia. Activation-dysfunction-injury, the protective role of simvastatin. *Vascul. Pharmacol.* **38,** 275–282
33. Fivaz, M., Vilbois, F., Thurnheer, S., Pasquali, C., Abrami, L., Bickel, P. E., Parton, R. G., and van der Goot, F. G. (2002) Differential sorting and fate of endocytosed GPI-anchored proteins. *EMBO J.* **21,** 3989–4000
34. Dermine, J. F., Duclos, S., Garin, J., St-Louis, F., Rea, S., Parton, R. G., and Desjardins, M. (2001) Flotillin-1-enriched lipid raft domains accumulate on maturing phagosomes. *J. Biol. Chem.* **276,** 18507–18512
35. Pietiäinen, V. M., Marjomäki, V., Heino, J., and Hyypiä, T. (2005) Viral entry, lipid rafts and caveosomes. *Ann. Med.* **37,** 394–403
36. Presley, T., Vedam, K., Velayutham, M., Zweier, J. L., and Ilangovan, G. (2008) Activation of Hsp90-eNOS and increased NO generation attenuate respiration of hypoxia-treated endothelial cells. *Am. J. Physiol. Cell Physiol.* **295,** C1281–C1291
37. Fontana, J., Fulton, D., Chen, Y., Fairchild, T. A., McCabe, T. J., Fujita, N., Tsuruo, T., and Sessa, W. C. (2002) Domain mapping studies reveal that the M domain of Hsp90 serves as a molecular scaffold to regulate Akt-dependent phosphorylation of endothelial nitric oxide synthase and NO release. *Circ. Res.* **90,** 866–873
38. Maron, B. A., and Michel, T. (2012) Subcellular localization of oxidants and redox modulation of endothelial nitric oxide synthase. *Circ. J.* **76,** 2497–2512
39. Chen, W., Druhan, L. J., Chen, C. A., Hemann, C., Chen, Y. R., Berka, V., Tsai, A. L., and Zweier, J. L. (2010) Peroxynitrite induces destruction of the tetrahydrobiopterin and heme in endothelial nitric oxide synthase. Transition from reversible to irreversible enzyme inhibition. *Biochemistry* **49,** 3129–3137
40. Jin, B. Y., Sartoretto, J. L., Gladyshev, V. N., and Michel, T. (2009) Endothelial nitric oxide synthase negatively regulates hydrogen peroxide-stimulated AMP-activated protein kinase in endothelial cells. *Proc. Natl. Acad. Sci. U.S.A.* **106,** 17343–17348
41. Conrad, P. A., Smart, E. J., Ying, Y. S., Anderson, R. G., and Bloom, G. S. (1995) Caveolin cycles between plasma membrane caveolae and the Golgi complex by microtubule-dependent and microtubule-independent steps. *J. Cell Biol.* **131,** 1421–1433
42. Brown, A. J., Mander, E. L., Gelissen, I. C., Kritharides, L., Dean, R. T., and Jessup, W. (2000) Cholesterol and oxysterol metabolism and subcellular distribution in macrophage foam cells. Accumulation of oxidized esters in lysosomes. *J. Lipid Res.* **41,** 226–237
43. Blair, A., Shaul, P. W., Yuhanna, I. S., Conrad, P. A., and Smart, E. J. (1999) Oxidized low density lipoprotein displaces endothelial nitric-oxide synthase (eNOS) from plasmalemmal caveolae and impairs eNOS activation. *J. Biol. Chem.* **274,** 32512–32519
44. Fernandes, R., Hosoya, K., and Pereira, P. (2011) Reactive oxygen species downregulate glucose transport system in retinal endothelial cells. *Am. J. Physiol. Cell Physiol.* **300,** C927–C936
45. Cuddy, L. K., Gordon, A. C., Black, S. A., Jaworski, E., Ferguson, S. S., and Rylett, R. J. (2012) Peroxynitrite donor SIN-1 alters high-affinity choline transporter activity by modifying its intracellular trafficking. *J. Neurosci.* **32,** 5573–5584
46. Heare, T., Alp, N. J., Priestman, D. A., Kulkarni, A. B., Qasba, P., Butters,

T. D., Dwek, R. A., Clarke, K., Channon, K. M., and Platt, F. M. (2007) Severe endothelial dysfunction in the aorta of a mouse model of Fabry disease; partial prevention by *N*-butyldeoxynojirimycin treatment. *J. Inherit. Metab. Dis.* **30,** 79–87

47. Bodary, P. F., Shen, Y., Vargas, F. B., Bi, X., Ostenso, K. A., Gu, S., Shayman, J. A., and Eitzman, D. T. (2005) α-Galactosidase A deficiency accelerates atherosclerosis in mice with apolipoprotein E deficiency. *Circulation* **111,** 629–632
48. Rombach, S. M., Twickler, T. B., Aerts, J. M., Linthorst, G. E., Wijburg, F. A., and Hollak, C. E. (2010) Vasculopathy in patients with Fabry disease. Current controversies and research directions. *Mol. Genet. Metab.* **99,** 99–108